plants

Article

Lead Immobilization in Soil and Uptake Reduction in *Brassica chinensis* Using Sepiolite-Supported Manganese Ferrite

Fengzhuo Geng [1,†], Yaping Lyu [2,†], Liansheng Ma [1], Yin Zhou [1], Jiayue Shi [1], Roland Bol [3], Peng Zhang [2], Iseult Lynch [4] and Xiuli Dang [1,*]

1 College of Land and Environment, National Engineering Research Center for Efficient Utilization of Soil and Fertilizer Resources, Key Laboratory of Arable Land Conservation in Northeast China, Ministry of Agriculture and Rural Affairs, Shenyang Agricultural University, Shenyang 110866, China; 2024220452@stu.syau.edu.cn (F.G.); ss15032928639@163.com (L.M.); zhouy20252025@163.com (Y.Z.); Sjy020517@163.com (J.S.)
2 Department of Environmental Science and Engineering, University of Science and Technology of China, Hefei 230026, China; 13001012362@163.com (Y.L.); zhangpeng1987@ustc.edu.cn (P.Z.)
3 Institute of Bio- and Geosciences, Agrosphere (IBG-3), Forschungszentrum Jülich GmbH, 52425 Jülich, Germany; r.bol@fz-juelich.de
4 School of Geography, Earth and Environmental Sciences, University of Birmingham, Edgbaston, Birmingham B15 2TT, UK; i.lynch@bham.ac.uk
* Correspondence: dxl@syau.edu.cn; Tel.: +86-136-0492-2085
† These authors contributed equally to this work.

Abstract

Lead (Pb) in soil poses serious environmental and health risks, and its removal requires complex and costly treatment methods to meet strict regulatory standards. To effectively address this challenge, innovative and efficient techniques are essential. Sepiolite-supported $MnFe_2O_4$ ($MnFe_2O_4$/SEP) composites were synthesized via a chemical co-precipitation method. The effects of $MnFe_2O_4$/SEP on soil pH, cation exchange capacity (CEC), available Pb content, Pb^{2+} uptake, and the activities of antioxidant enzymes in *Brassica chinensis* (Pak Choi) were examined. $MnFe_2O_4$/SEP showed superior Pb^{2+} adsorption compared to SEP alone, fitting Langmuir models, Dubinin-Radushkevich (D-R) models, Temkin models and pseudo-second-order kinetics. The maximum adsorption capacities at 298, 308, and 318 K were 459, 500 and 549 $mg{\cdot}g^{-1}$, respectively. XPS analysis indicated that chemisorption achieved through ion exchange between Pb^{2+} and H^+ was the main mechanism. $MnFe_2O_4$/SEP increased the soil pH by 0.2–1.5 units and CEC by 18–47%, while reducing available Pb by 12–83%. After treatment with $MnFe_2O_4$/SEP, acid-extractable and reducible Pb in the soil decreased by 14% and 39%, while oxidizable and residual Pb increased by 26% and 21%, respectively. In *Brassica chinensis*, $MnFe_2O_4$/SEP reduced Pb^{2+} uptake by 76%, increased chlorophyll content by 36%, and decreased malondialdehyde (MDA) levels by 36%. The activities of antioxidant enzymes—superoxide dismutase (SOD), peroxidase (POD), and catalase (CAT)—were decreased by 29%, 38% and 17%, respectively. These findings demonstrate that $MnFe_2O_4$/SEP is an efficient Pb^{2+} adsorbent that immobilizes Pb in soil mainly through ion exchange, thereby providing a highly effective strategy for remediating Pb-contaminated soils and improving plant health.

Keywords: manganese ferrite nanoparticles ($MnFe_2O_4$ NPs); adsorption; soil remediation; Pak Choi; nano-composite; lead toxicity

check for updates

Academic Editor: Monica Ruffini Castiglione

Received: 25 August 2025
Revised: 1 October 2025
Accepted: 3 October 2025
Published: 5 October 2025

Citation: Geng, F.; Lyu, Y.; Ma, L.; Zhou, Y.; Shi, J.; Bol, R.; Zhang, P.; Lynch, I.; Dang, X. Lead Immobilization in Soil and Uptake Reduction in *Brassica chinensis* Using Sepiolite-Supported Manganese Ferrite. *Plants* **2025**, *14*, 3077. https://doi.org/10.3390/plants14193077

Copyright: © 2025 by the authors. Licensee MDPI, Basel, Switzerland. This article is an open access article distributed under the terms and conditions of the Creative Commons Attribution (CC BY) license (https://creativecommons.org/licenses/by/4.0/).

1. Introduction

In recent decades, rapid economic development has accelerated the release of heavy metals, particularly lead (Pb), into the environment. It is estimated that approximately 783,000 tons of Pb have been discharged globally, with soils acting as the ultimate sink and consequently experiencing significant contamination [1]. A national survey of soil pollution in China conducted from 2005 to 2013 showed that inorganic pollution accounted for the largest proportion (16.1%) of environmental contamination among all types. Furthermore, according to the latest survey by the Ministry of Ecology and Environment (2023–2024), 7.2% of China's farmland soil exceeds the Pb^{2+} limits set by national standards. Vegetables play an important role in the Chinese diet, and Pak Choi (*Brassica chinensis*), a common leafy green, is widely consumed. However, Pb^{2+} is readily absorbed by *Brassica chinensis* from contaminated soil and transferred to humans through the food chain, posing serious health risks [2,3]. Notably, Pb^{2+} exposure can severely impair the nervous system and vital organs, with children being particularly vulnerable to its detrimental effects on growth and development [4]. Therefore, developing a simple and low-cost method to remove Pb^{2+} from soil has become a critical issue. Chemical precipitation, electrochemical methods, ion exchange and adsorption methods are the popular technologies for remediation of Pb-contaminated farmland [5]. Among these methods, adsorption is the preferred approach for remediating Pb-contaminated farmland due to its high efficiency and low cost [6]. Hence, the development of highly effective adsorbents for heavy metal removal is a significant trend in current environmental research, with a variety of materials such as carbon-based compounds, nanoparticles, and clay minerals being investigated for their ability to remove heavy metals from wastewater and soil [7–9].

Manganese ferrite nanoparticles ($MnFe_2O_4$ NPs) have gained prominence due to their remarkable physicochemical, optical, and magnetic features, including low magnetic loss, high permeability, and robust chemical stability. Un-agglomerated $MnFe_2O_4$ has a large specific surface area due to its nanoscale, and a large number of hydroxyl groups on the surface make it a potential substrate for Pb^{2+} adsorption [10]. However, the magnetic nature of $MnFe_2O_4$ NPs often leads to their agglomeration, which makes the actual surface area for adsorption, and the absorption efficiency much lower than the theoretical value [11]. This issue is typically addressed by using carbon-based or silica-based materials as stabilizing supports for $MnFe_2O_4$ NPs to reduce their agglomeration potential [12]. Loading magnetic $MnFe_2O_4$ onto a sludge biochar composite has been demonstrated to effectively prevent the agglomeration of $MnFe_2O_4$ and improve the adsorption efficiency of Pb^{2+} [13].

Natural clay minerals are aluminosilicates with a layered structure. Common clay minerals include zeolite, sepiolite (SEP) and montmorillonite, which are natural materials with adsorption properties for Pb^{2+} [14]. SEP, in particular, stands out as a fibrous sheet-structured silicate clay mineral, rich in silicon and magnesium. The lamellar fiber structure of SEP has a large specific surface area, which is not only an excellent natural material for adsorption of Pb^{2+}, but also an ideal carrier for nanomaterials. Fu et al. (2015) successfully prepared SEP-supported nano-zero-valent iron for efficient removal of Cr^{6+} and Pb^{2+} from groundwater [15]. The results showed that the agglomeration phenomenon of nano-zero-valent iron after loading was reduced, and the removal rate of Cr^{6+} and Pb^{2+} in water was increased. Therefore, SEP is a potential support for $MnFe_2O_4$ NPs. The synergy between $MnFe_2O_4$ and SEP in a composite form is anticipated to not only preserve but also amplify the inherent adsorption qualities of each individual component, harnessing the best of both worlds for improved efficacy in heavy metal removal.

In this study, a sepiolite-supported manganese ferrite nanoparticles ($MnFe_2O_4$/SEP) composite magnetic material was prepared and characterized by scanning electron microscope with energy dispersive spectroscopy (SEM–EDS), X-ray diffraction (XRD), Fourier

Transform infrared (FT-IR) spectroscopy and X-ray Photoelectron Spectroscopy (XPS). The adsorption behavior and properties of Pb^{2+} in water were studied under the conditions of different material dosage, pH, adsorption temperature and adsorption time. In addition, through adsorption kinetics, adsorption thermodynamics calculations, and isothermal adsorption fitting, combined with XPS characterization, the adsorption mechanism for Pb^{2+} was explored. Finally, the remediation effects of $MnFe_2O_4$/SEP in soil were evaluated by measuring the Pb availability, Pb^{2+} content, enzyme activities and the antioxidative responses in the plant *Brassica chinensis* grown in the Pb-contaminated soil.

2. Results and Discussion

2.1. Adsorbent Characterization

The morphologies and elemental compositions of raw SEP and $MnFe_2O_4$/SEP are shown in Figure S1. SEP exhibited a typical fibrous lamellar structure with a smooth surface (Figure S1a) and was mainly composed of Ca, Mg, O, and Si (Figure S1c). After modification, the surface became rough with granular deposits, while $MnFe_2O_4$ aggregation was effectively prevented (Figure S1b). Energy spectrum analysis confirmed the presence of Mn and Fe in the composite (Figure S1d and Table S2). The content ratio of the two elements was 1:2, and compared with SEP, their contents increased by 11% and 22% respectively, indicating successful $MnFe_2O_4$ loading. The specific surface area increased from 34.04 to 112.61 $m^2 \cdot g^{-1}$ (Table S1), providing 3.3 times more binding sites for heavy metals. These improvements suggest that $MnFe_2O_4$/SEP has strong potential as an efficient Pb^{2+} adsorbent. XRD analysis confirmed the crystal structures of SEP, $MnFe_2O_4$, and $MnFe_2O_4$/SEP (Figure S1e). Reflections at 7.25°, 27.91°, 39.86°, and 43.64° corresponded to SEP (JCPDS 26-1226), while additional peaks at 34.88°, 36.47°, 52.59°, and 61.51° (JCPDS 38-0430) verified the presence of $MnFe_2O_4$. FT-IR spectra (Figure S1f) further confirmed $MnFe_2O_4$ loading, with Mn–O (680 cm^{-1}) and Fe–O (484 cm^{-1}) vibrations observed. The decreased –OH signal at 3673 cm^{-1} and the broadened band at 3000–3450 cm^{-1} suggested loss of bonded water and formation of new functional groups [16], which are expected to enhance the cation exchange capacity and Pb^{2+} adsorption [17].

2.2. Adsorption Properties of $MnFe_2O_4$/SEP

The adsorption behavior of Pb^{2+} by SEP and $MnFe_2O_4$/SEP was strongly influenced by pH (Figure 1a). With increasing pH, both adsorption capacity and removal efficiency increased due to the reduced competition between H^+ and Pb^{2+} for active sites [18]. Maximum adsorption was achieved at pH 6, where $MnFe_2O_4$/SEP reached nearly 100% removal, significantly outperforming SEP, indicating more available binding sites in the composite. Adsorbent dosage also affected Pb^{2+} removal (Figure 1b). At lower dosages, adsorption approached maximum capacity, whereas higher dosages mainly improved removal efficiency [19]. An optimal dosage of 0.6 $g \cdot L^{-1}$ $MnFe_2O_4$/SEP achieved 92.68% Pb^{2+} removal, outperforming bare SEP. Isothermal adsorption results further demonstrated that Pb^{2+} uptake by $MnFe_2O_4$/SEP increased with initial concentration and temperature, reaching equilibrium above 500 $mg \cdot L^{-1}$ (Figure 1c). Langmuir isotherm fitting provided the best description of the process, with theoretical maximum adsorption capacities of 458, 500, and 549 $mg \cdot g^{-1}$ at 298, 308, and 318 K, respectively (Table 1), confirming monolayer chemisorption as the dominant mechanism. D-R model fitting yielded characteristic adsorption energies (E) of 0.37, 0.43 and 0.49 $kJ \cdot mol^{-1}$ at 298, 308, and 318 K (Table 1). Since all values were below 8 $kJ \cdot mol^{-1}$, the adsorption process can be attributed to physical adsorption [20]. In contrast, the Temkin model fitting produced adsorption heat constants (b) of 28.01, 30.06, and 31.80 $kJ \cdot mol^{-1}$ at 298, 308, and 318 K, respectively. These values fall within the range of 20–40 $kJ \cdot mol^{-1}$, suggesting the involvement of chemical adsorption [21]. Taken together, these findings indicate that the adsorption of Pb^{2+} by $MnFe_2O_4$/SEP is governed by the combined contributions of both physical and chemical adsorption.

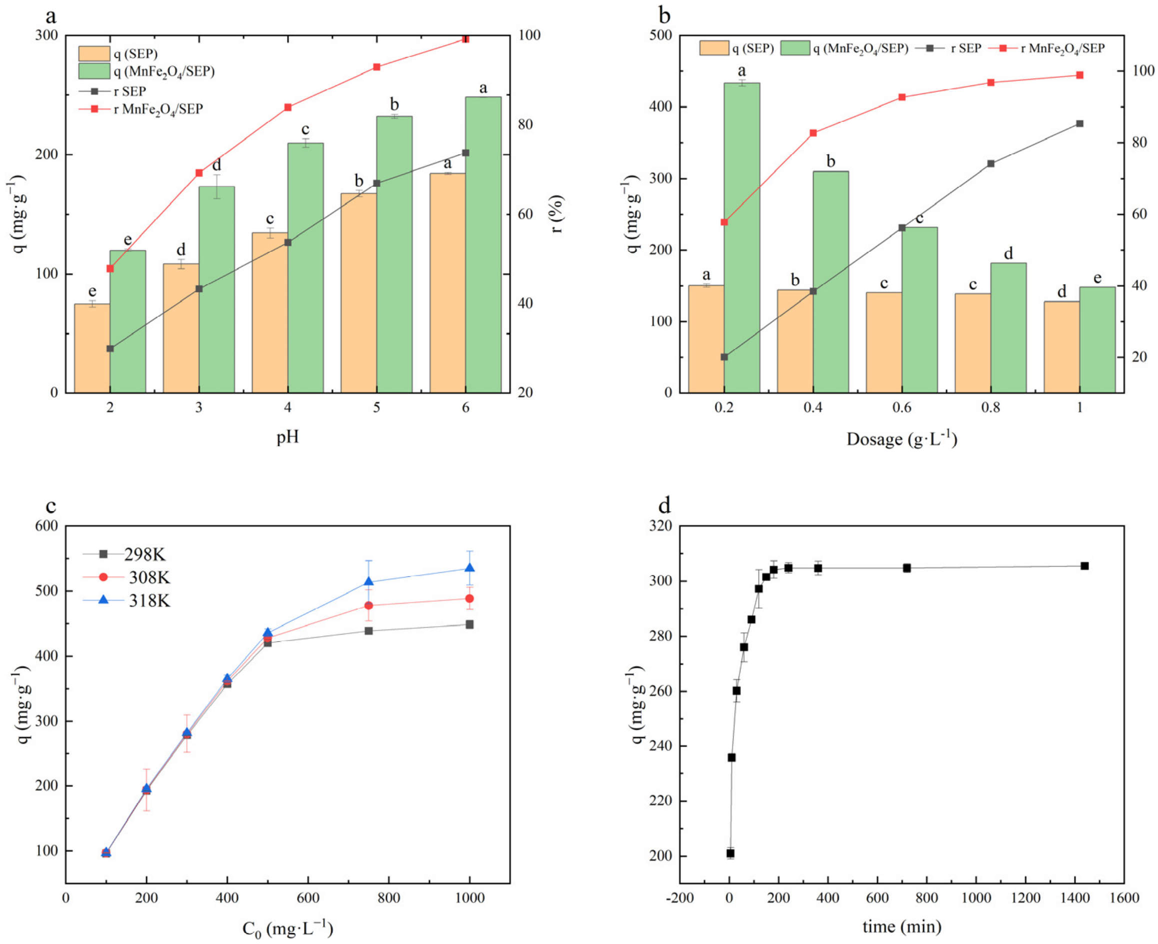

Figure 1. Effect of pH (**a**), dosage (**b**), initial concentration and temperature (**c**) and time (**d**) on the Pb^{2+} adsorption quantity (q) and removal rate (r) by SEP and $MnFe_2O_4$/SEP. Data are presented as mean ± SE (n = 3). Different lowercase letters indicate significant difference between different treatments ($p < 0.05$).

Table 1. Langmuir, Dubinin-Radushkevich and Temkin parameters for Pb^{2+} adsorption onto $MnFe_2O_4$/SEP.

T(K)	Langmuir			D-R			Temkin		
	q_{max} ($mg \cdot g^{-1}$)	K_L ($L \cdot mg^{-1}$)	R^2	q_{max} ($mg \cdot g^{-1}$)	E ($kJ \cdot mol^{-1}$)	R^2	A ($L \cdot mg^{-1}$)	b ($kJ \cdot mol^{-1}$)	R^2
298	458.72	0.09	0.99	368.5	0.37	0.88	2.26	28.01	0.91
308	500.00	0.08	0.99	380.0	0.43	0.86	1.94	30.06	0.95
318	549.45	0.07	0.99	413.5	0.49	0.87	1.83	31.80	0.97

2.3. Adsorption Kinetics

The kinetic effect of Pb^{2+} adsorption by the adsorbent was investigated through studies on the adsorption process at different time intervals. As shown in Figure 1d, the Pb^{2+} adsorption capacity of $MnFe_2O_4$/SEP increased rapidly within 1 h, slowed between 1–3 h, and reached equilibrium after 3 h. Initially, favorable conditions—including abundant adsorption sites on $MnFe_2O_4$/SEP and high Pb^{2+} concentration—caused rapid adsorption within the first hour. With time extension (2–3 h), reduced surface sites decreased pore diffusion rates, but electrostatic repulsion existed between the unadsorbed Pb^{2+} in the solution and the Pb^{2+} already bound to the surface of $MnFe_2O_4$/SEP [22,23] until equilibrium was achieved with complete site occupation. Kinetic fitting results (Figure S2, Table S3) showed the pseudo-second-order model best described the adsorption process. This model, which encompasses both internal diffusion and surface adsorption of the composite, indicates that the Pb^{2+} adsorption mechanism of $MnFe_2O_4$/SEP results from multiple combined effects [24].

2.4. Thermodynamic Study

By analyzing the adsorption process of Pb^{2+} by $MnFe_2O_4$/SEP at 298, 308 and 318 K, the thermodynamic behavior of adsorption was further determined. The thermodynamic fitting results are shown in Figure 2. The results showed that the process for $MnFe_2O_4$/SEP adsorption of Pb^{2+} was endothermic (ΔH was 11.91 kJ·mol^{-1}) and that increasing the temperature increased the disorder of the adsorption system and thus increased the amount of Pb^{2+} adsorbed by $MnFe_2O_4$/SEP. The adsorption process was spontaneous, as indicated by the negative ΔG values at all three temperatures (−25.38, −26.63, and −27.88 kJ·mol^{-1}, respectively). Moreover, the ΔG values were all below 50 kJ·mol^{-1}, suggesting that the removal of Pb^{2+} by $MnFe_2O_4$/SEP was primarily controlled by chemical interactions [25]. Previously, Langmuir fitting indicated that adsorption mainly occurs on the material surface. The characteristic adsorption energy E from D-R fitting (E < 8 kJ·mol^{-1}) confirms physical interactions, while the adsorption heat constant b from Temkin fitting (20–40 kJ·mol^{-1}) suggests chemical interactions—together proving a physico-chemical synergistic adsorption process. Pseudo-first-order kinetics shows that Pb^{2+} physically diffuses to the material surface in the initial adsorption stage, and pseudo-second-order kinetics indicates chemical adsorption dominates the process. Based on the above comprehensive analysis, the adsorption mechanism of $MnFe_2O_4$/SEP can be summarized as a spontaneous process dominated by chemical adsorption with physical adsorption as a supplement, under the mode of monolayer surface adsorption.

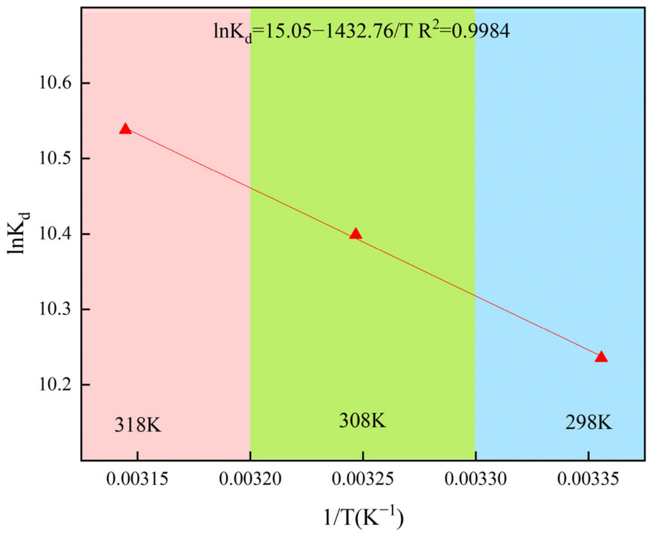

Figure 2. Van't Hoff plot for the adsorption of Pb^{2+} onto $MnFe_2O_4$/SEP as a function of temperature.

2.5. Reusability Assessment

The regeneration ability of $MnFe_2O_4$/SEP was evaluated by repeating the adsorption–desorption cycle five times. As shown in Figure 3, the Pb^{2+} removal rate and the $MnFe_2O_4$/SEP recovery rate gradually decreased with an increasing number of adsorption–desorption cycles. There are two possible reasons for this; one is the loss of adsorbent in the process of the adsorption and desorption cycle, and the other is that a small number of adsorption sites may be lost in the process of desorption, resulting in the reduction of removal rate over time. During the five cycles, the gap between the removal rate of Pb^{2+} and the recovery rate of the material became larger and larger, and the main reason for the decrease of Pb^{2+} removal rate was the inactivation of adsorption sites on the surface of $MnFe_2O_4$/SEP. However, after the fifth cycle, the removal rate still reached 85.4%. Therefore, $MnFe_2O_4$/SEP has a certain inherent stability and is expected to become a new kind of soil treatment material which is easy to prepare and economical.

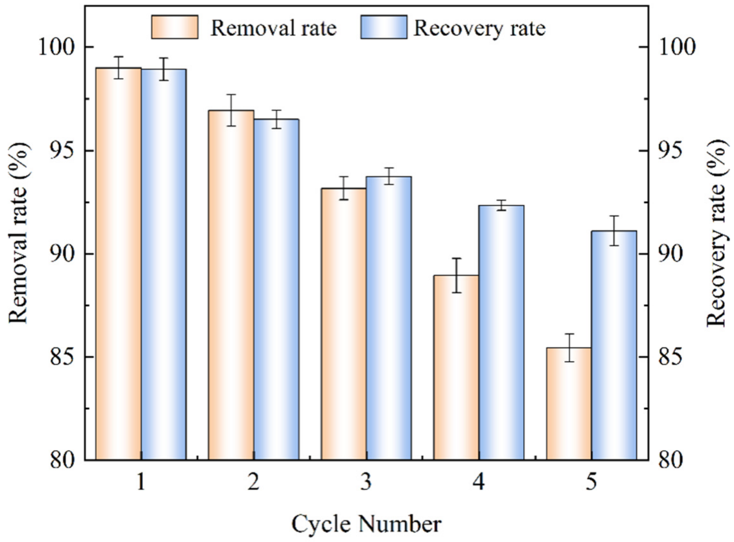

Figure 3. Removal rate of Pb^{2+} and recovery rate of $MnFe_2O_4$/SEP after five adsorption–desorption cycles using $MnFe_2O_4$/SEP. Data are presented as mean ± SD with n = 3 independent replicates.

2.6. Adsorption Mechanism

The XPS full spectrum scanning results are shown in Figure 4a. In addition to Mg, Ca, Fe, Mn, O, Si, and other elements contained in the material itself, the adsorbed material showed the characteristic absorption peaks of Pb 4d and Pb 4f, indicating that Pb^{2+} has been successfully bound to the surface of $MnFe_2O_4$/SEP. Figure 4b shows the high-resolution energy spectrum of Pb 4f, revealing that the shift of characteristic peaks relative to the standard binding energy is consistent with the characteristic adsorption energy E (average value of 0.4 $kJ \cdot mol^{-1}$) calculated by the D-R isotherm model and the adsorption heat constant b (average value of 30 $kJ \cdot mol^{-1}$) from the Temkin model. This consistency confirms that both physical and chemical interactions coexist in the adsorption process. The characteristic spectra of the O 1s orbitals of $MnFe_2O_4$/SEP and Pb-$MnFe_2O_4$/SEP are shown in Figure 4c,d. The characteristic peaks of O 1s can be fitted to five forms of O [26]. The peak area of metal hydroxide decreased significantly after adsorption, and the peak area of metal oxide increased significantly which may be caused by Pb^{2+} replacing H^+ at the adsorption site. Before and after adsorption, the binding energy of Si-O bonds shifted. This shift may be attributed to the replacement of H in Si-OH groups by part of Pb, which forms Si-O-Pb bonds. The formation of Si-O-Pb bonds causes the binding energy of Si-O bonds to shift, thereby enabling Pb to be complexed on the surface and within the pores of the composite material. This is consistent with the indication of the pseudo-second-order kinetic model that chemical adsorption is the rate-limiting step, and it is consistent with the characteristics of monolayer adsorption on uniform active sites revealed by the Langmuir model, suggesting that the chemical complexation between Pb^{2+} and active sites constitutes the core mechanism of the adsorption process. In addition, the pseudo-first-order kinetic model reveals the existence of a physical diffusion process in the initial stage of adsorption, which is corroborated by the physical interaction reflected by the D-R model. This indicates that Pb^{2+} first diffuses to the material surface through physical attraction, laying the foundation for subsequent chemical adsorption.

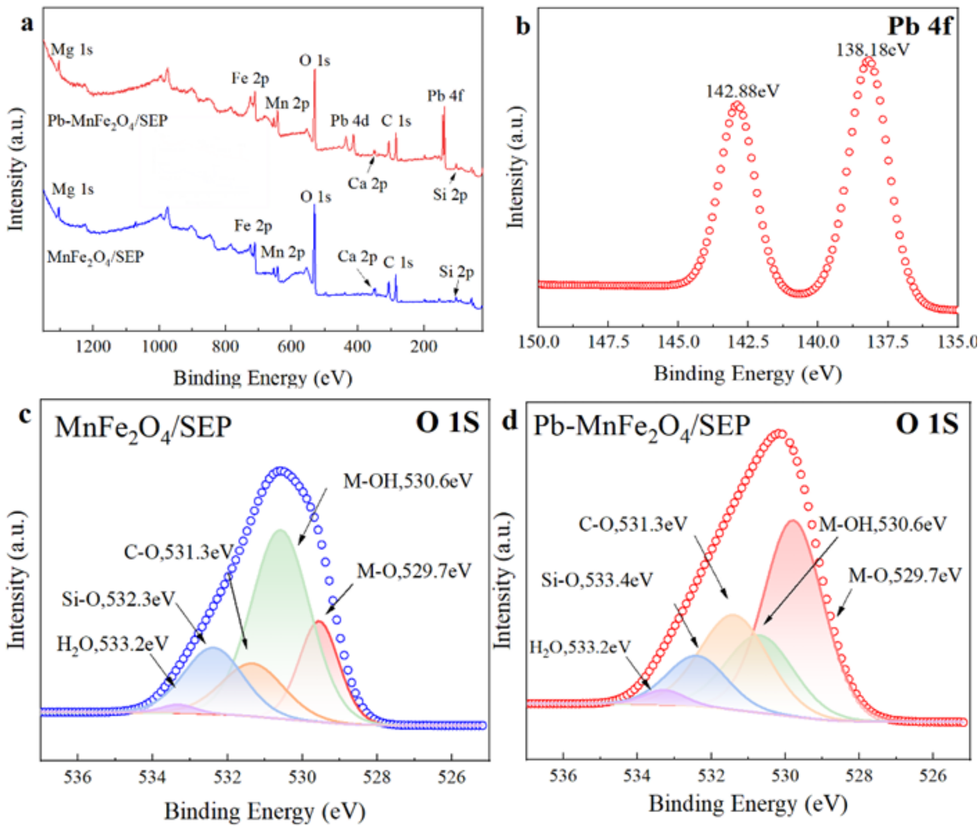

Figure 4. Characterization of the binding mechanisms, (**a**) XPS survey spectra of $MnFe_2O_4$/SEP before and after Pd^{2+} adsorption, (**b**) high-resolution XPS spectra of Pb4f, (**c**,**d**) fitting results of O1s before and after Pb^{2+} adsorption.

In summary, the adsorption mechanism of Pb^{2+} from aqueous solutions by the $MnFe_2O_4$/SEP composite mainly involves physical adsorption and chemical adsorption, with chemical adsorption being dominant. Ion exchange is primarily manifested in the complexation of Pb^{2+} on the composite surface by the M-OH and Si-OH groups on the composite surface.

$$\text{Si-OH} + Pb^{2+} = [(\text{Si-O})Pb]^{+} + H^{+} \quad (1)$$

$$2\text{Si-OH} + Pb^{2+} = (\text{Si-O})_2Pb + 2H^{+} \quad (2)$$

$$\text{M-OH} + Pb^{2+} = [(\text{M-O})Pb]^{+} + H^{+} \quad (3)$$

$$2\text{M-OH} + Pb^{2+} = (\text{M-O})_2Pb + 2H^{+} \quad (4)$$

2.7. *Application of $MnFe_2O_4$/SEP in Pb-Contaminated Soil*

2.7.1. Effects of $MnFe_2O_4$/SEP on Soil pH, CEC, and Available Pb Content

As shown in Figure 5, $MnFe_2O_4$/SEP increased soil pH and cation exchange capacity (CEC) in a dose-dependent manner. Compared with the control (CK), soil pH rose by 0.2–1.5 units with increasing $MnFe_2O_4$/SEP, reaching 7.4 at 40 $g \cdot kg^{-1}$ ($p < 0.05$). This was because SEP is weakly alkaline, and as the amount of SEP added increased, it resulted in a significant increase in soil pH [27]. Soil CEC also increased by 18–47%, likely due to the material's high surface area [28]. Correspondingly, the content of available Pb decreased by 12–83% with increasing $MnFe_2O_4$/SEP. This reduction can be attributed to adsorption and ion exchange on $MnFe_2O_4$/SEP. Sequential extraction showed that $MnFe_2O_4$/SEP decreased acid-extractable and reducible Pb fractions while increasing oxidizable and residual fractions, indicating a transformation of Pb^{2+} into more stable, less bioavailable forms and thus reducing its uptake by plants [9].

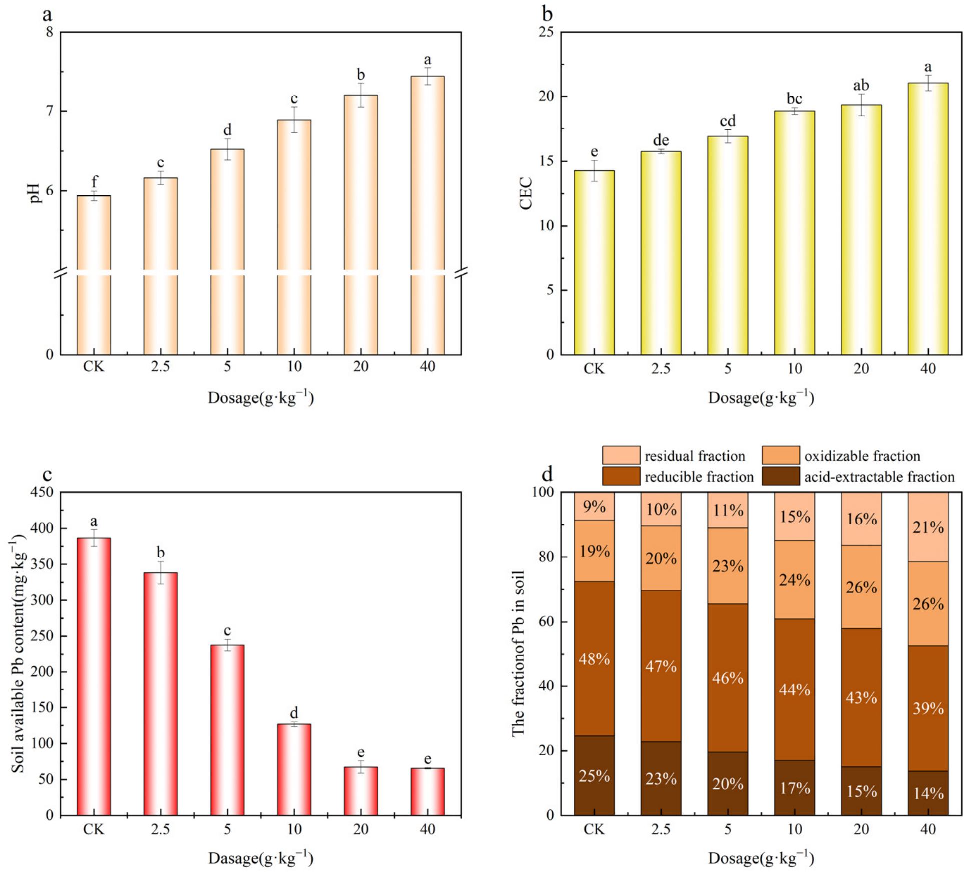

Figure 5. Effects of addition of different amounts of $MnFe_2O_4$/SEP on (**a**) soil pH, (**b**) soil CEC, (**c**) available Pb content, and (**d**) soil Pb fraction. Data are presented as mean ± SE (n = 3). Different lowercase letters indicate significant difference between different treatments ($p < 0.05$).

2.7.2. Effect of $MnFe_2O_4$/SEP on Pb^{2+} Uptake, Chlorophyll Content and Yield in *Brassica chinensis*

As shown in Figure 6a, exogenous Pb addition (300, 600, and 900 mg·kg^{-1}) significantly increased Pb uptake by *Brassica chinensis* compared with the control (CK), with Pb contents rising by 0.2, 0.4, and 0.6 mg·kg^{-1}, respectively ($p < 0.05$). In contrast, $MnFe_2O_4$/SEP application reduced Pb uptake by 61%, 72%, and 76% under the corresponding Pb levels ($p < 0.05$). Pb stress also decreased chlorophyll content by 21%, 29%, and 36% (Figure 6b), while $MnFe_2O_4$/SEP increased it by 14%, 36%, and 36%, respectively, compared with treatments without the amendment. Compared with CK, Pb addition in soil significantly reduced the fresh weight of Brassica chinensis ($p < 0.05$). However, $MnFe_2O_4$/SEP treatment led to a significant increase of 15–54% in fresh weight compared with the non-$MnFe_2O_4$/SEP group ($p < 0.05$) (Figure 6c). These results indicate that $MnFe_2O_4$/SEP effectively lowers bioavailable Pb in soil, mitigates Pb-induced cellular damage, and enhances chlorophyll levels in *Brassica chinensis* [29].

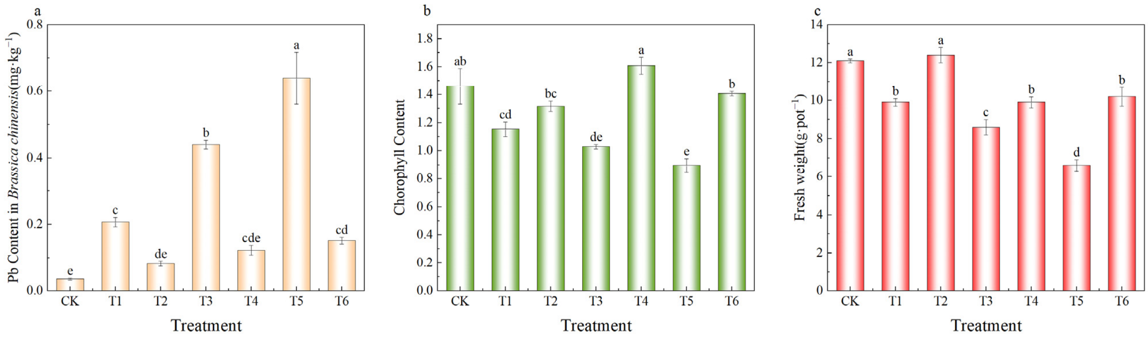

Figure 6. Effect of $MnFe_2O_4$/SEP on (**a**) Pb^{2+} uptake, (**b**) chlorophyll content in *Brassica chinensis* and (**c**) fresh weight of *Brassica chinensis*. Data are presented as means ± SE (n = 3). Different lowercase letters indicate significant difference between different treatments (p < 0.05). The treatments applied include: CK-control, T1—300 $mg \cdot kg^{-1}$ Pb^{2+}, T2—300 $mg \cdot kg^{-1}$ Pb^{2+} plus 20 $g \cdot kg^{-1}$ $MnFe_2O_4$/SEP, T3—600 $mg \cdot kg^{-1}$ Pb^{2+}, T4—600 $mg \cdot kg^{-1}$ Pb^{2+} plus 20 $g \cdot kg^{-1}$ $MnFe_2O_4$/SEP, T5—900 $mg \cdot kg^{-1}$ Pb^{2+}, and T6—900 $mg \cdot kg^{-1}$ Pb^{2+} plus 20 $g \cdot kg^{-1}$ $MnFe_2O_4$/SEP.

2.7.3. Effect of $MnFe_2O_4$/SEP on MDA and Antioxidant Enzymes System in *Brassica chinensis*

As shown in Figure 7, Pb stress significantly increased MDA content in *Brassica chinensis* by 46–71% compared with the control (CK), indicating elevated lipid peroxidation. Application of $MnFe_2O_4$/SEP reduced MDA levels by 29–36%, approaching CK levels. Similarly, Pb exposure elevated the activities of antioxidant enzymes SOD, POD, and CAT, while $MnFe_2O_4$/SEP treatment effectively decreased these activities toward control levels (SOD: 24–29%; POD: 19–38%; CAT: 3–17%).

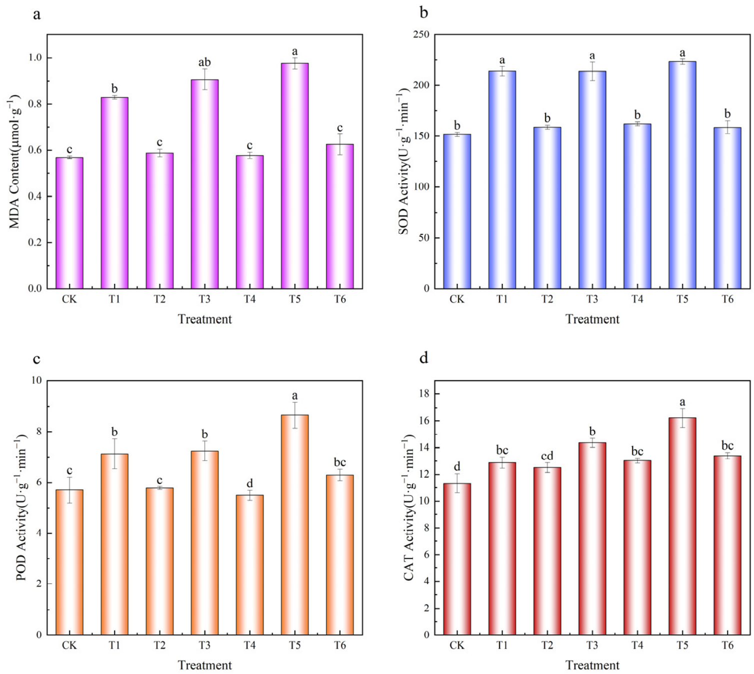

Figure 7. Effect of $MnFe_2O_4$/SEP on the activity of antioxidant enzymes induced in response to Pb^{2+} taken up from soil. (**a**) MDA content of *Brassica chinensis*, (**b**) SOD activity of *Brassica chinensis*, (**c**) POD activity of *Brassica chinensis*, (**d**) CAT activity of *Brassica chinensis*. Data are presented as mean ± SE (n = 3). Different lowercase letters indicate statistically significant differences between different treatments (p < 0.05). The treatments applied include: CK- control, T1—300 $mg \cdot kg^{-1}$ Pb^{2+}, T2—300 $mg \cdot kg^{-1}$ Pb^{2+} plus 20 $g \cdot kg^{-1}$ $MnFe_2O_4$/SEP, T3—600 $mg \cdot kg^{-1}$ Pb^{2+}, T4—600 $mg \cdot kg^{-1}$ Pb^{2+} plus 20 $g \cdot kg^{-1}$ $MnFe_2O_4$/SEP, T5—900 $mg \cdot kg^{-1}$ Pb^{2+}, and T6—900 $mg \cdot kg^{-1}$ Pb^{2+} plus 20 $g \cdot kg^{-1}$ $MnFe_2O_4$/SEP.

Under Pb stress, plants are compelled to generate reactive oxygen species (ROS) such as O^{2-}, OH^-, NO^-, which disrupt the antioxidant defense system. Plants can activate their intrinsic defense mechanisms to scavenge these products and mitigate oxidative damage by enhancing the activities of key antioxidant enzymes, including SOD, CAT, and POD [30,31]. When plants are under environmental stress, MDA is produced through lipid peroxidation in cell membranes and cytoplasm. Higher MDA content indicates more severe stress damage in plants. In this study, $MnFe_2O_4$/SEP application reduced the Pb content in *Brassica chinensis*, alleviated the toxic effects of free radicals and ROS to plant cells and tissues, and enhanced SOD, CAT, and POD activities, thereby mitigating Pb stress-induced damage [32].

3. Materials and Methods

3.1. Sample Preparation and Characterization

Brown soil (0–20 cm depth) was collected from Dalian Village, Sujiatun District, Shenyang, Liaoning Province. Samples were air-dried, ground, sieved through a 20-mesh sieve, and analyzed for physicochemical properties. Soil pH was measured according to ISO 10390 [33] using a glass electrode in a 1:2.5 soil-water suspension, and organic matter by the $K_2Cr_2O_7$ external heating method [34]. Pb, Fe, and Mn contents were determined by acid digestion method [35]. Results showed pH 5.8 ± 0.1, organic matter 34.4 ± 1.5 $g \cdot kg^{-1}$, Pb 34.7 ± 2.1 $mg \cdot kg^{-1}$, Fe 4.1 ± 0.3 $g \cdot kg^{-1}$, and Mn 1.0 ± 0.1 $g \cdot kg^{-1}$. SEP was purchased from Sinopharm Chemical Reagent Co., Ltd., Shanghai, China. *Brassica chinensis* seeds were purchased from Xinhai Agricultural Development Co., Ltd., Harbin, China.

3.2. Synthesis of $MnFe_2O_4$/SEP and Characterization

$MnFe_2O_4$/SEP was synthesized by co-precipitation [36]. Briefly, 0.1 $mol \cdot L^{-1}$ $MnSO_4 \cdot H_2O$ and 0.2 $mol \cdot L^{-1}$ $FeCl_3 \cdot 6H_2O$ were mixed at a molar ratio of 1:2 and stirred at 25 °C and 200 rpm for 30 min. The pH was adjusted to 10, followed by aging at 60 °C for 4 h. The resulting suspension was filtered through a 0.45 μm membrane, washed with distilled water, and dried to obtain magnetic $MnFe_2O_4$ nanoparticles. For $MnFe_2O_4$/SEP synthesis, SEP was incorporated into the precursor solution, and the same procedure was repeated. Preliminary adsorption tests with SEP: $MnFe_2O_4$ ratios of 1:2, 1:1, and 2:1 showed that the 1:1 ratio exhibited the highest performance (248 $mg \cdot g^{-1}$ adsorption capacity; 99% Pb^{2+} removal) and was therefore selected for subsequent experiments.

The morphologies and elemental compositions of SEP and $MnFe_2O_4$/SEP were examined by SEM equipped with EDS (ZEISS GeminiSEM 300 Carl Zeiss AG, Oberkochen, Germany). Surface area and pore size distribution were determined with a Micrometeritics ASAP 2460 (Micromeritics Instrument Corporation, Norcross, GA, USA). Mineral phases of SEP, $MnFe_2O_4$ and $MnFe_2O_4$/SEP were analyzed by XRD (Rigaku Ultima IV Rigaku Corporation, Tokyo, Japan) with a scanning range of 2θ = 5°~90° and a rate of 5 $° \cdot min^{-1}$. Surface functional groups of SEP and $MnFe_2O_4$/SEP were characterized by FT-IR (Thermo Scientific Nicolet iS50 Thermo Fisher Scientific Inc., Waltham, MA, USA) in the range of 400–4000 cm^{-1}. The chemical composition of $MnFe_2O_4$/SEP before and after Pb adsorption were further investigated by XPS (Thermo Scientific K-Alpha Thermo Fisher Scientific Inc., Waltham, MA, USA).

3.3. Adsorption Experiments: SEP and $MnFe_2O_4$/SEP Efficiency in Removal of Pb^{2+}

Batch experiments were performed to investigate Pb^{2+} removal by SEP and $MnFe_2O_4$/SEP. The effects of pH (2–6), adsorbent dosage (0.2–1.0 $g \cdot L^{-1}$), temperature (298–318 K), and initial Pb^{2+} concentration (100–1000 $mg \cdot L^{-1}$) were studied in 150 mL conical flasks at 180 rpm. Simulated Pb^{2+} solutions were prepared from analytical-grade Pb $(NO_3)_2$ in deionized water. For adsorption kinetics, 0.04 g of absorbent was added to 100 mL Pb^{2+} solutions of 500 mg·L^{-1}, and samples were collected at various time points within 24 h. After filtration through 0.45 μm syringe filters, Pb^{2+} concentrations were determined by atomic absorption spectrophotometry (Agilent240FS Agilent Technologies, Inc., Santa Clara, CA, USA). All experiments were performed in triplicate. Adsorption capacity calculations are detailed in the Supplemental Information (Text S1).

3.4. Regeneration and Reuse Efficiency of $MnFe_2O_4$/SEP

Regeneration and reuse were evaluated through repeated adsorption–desorption cycles. For adsorption, 0.5 g of $MnFe_2O_4$/SEP was dispersed in 100 mL Pb^{2+} solution (500 mg·L^{-1}) and stirred for 24 h. The mixture was filtered through a 0.45 μm syringe filter, and the adsorbent was dried at 105 °C for 24 h. Pb^{2+} concentrations before and after adsorption were measured by flame atomic absorption spectrometry (Agilent 240FS) to calculate removal rate efficiency. For desorption, the dried adsorbent was treated to 100 mL of 0.2 mol·L^{-1} EDTA-2Na solution for 24 h, filtered, and dried again. Pb^{2+} concentration in the desorption solution was measured, and the recovery rate was calculated as the ratio of desorbed Pb^{2+} to previously adsorbed Pb^{2+}. The adsorption–desorption cycle was repeated five times. Calculation details are provided in the Supplemental Information (Text S1).

3.5. Soil Incubation Experiment

Pb-contaminated soil was prepared by spiking with a Pb $(NO_3)_2$ to achieve 600 mg·kg^{-1}, simulating moderately contaminated farmland soil according to the Soil Environmental Quality Risk Control Standard for Agricultural Land (GB 15618-2018) [37], intervention range 400–1000 mg·kg^{-1}). The spiked soil was air-dried for 15 days and passed through a 20-mesh sieve. For incubation, 100 g of soil was thoroughly mixed with $MnFe_2O_4$/SEP at 0, 2.5, 5, 10, 20, and 40 g·kg^{-1}and transferred into 300 mL plastic bottles, with three replicates per treatment. Soil moisture was maintained at 60% of water holding capacity by periodic addition of deionized water over 30 days.

After incubation, the soil pH, CEC, available Pb, Pb fractionation, and total Pb were determined. CEC was measured by the $BaCl_2$-H_2SO_4 compulsive exchange method (ISO 11260, 2017) [9]. Available Pb was extracted using DTPA according to the Chinese National Standard GB/T 23739-2009 [38], Pb fractionation was determined via the European Community Bureau of Reference (BCR) sequential extraction procedure [39], and total Pb was measured by strong acid digestion (GB/T 17141-1997) [35].

3.6. Pot Experiments for Remediation Assessment

Simulated Pb-contaminated soils were prepared by spiking with $Pb(NO_3)_2$ to final concentrations of 300, 600, and 900 mg·kg^{-1}. Treatments included soils with or without 20 g·kg^{-1} $MnFe_2O_4$/SEP, with three replicates per treatment. The experimental design consisted of the following treatment: 300 mg·kg^{-1} Pb without $MnFe_2O_4$/SEP (T1), 300 mg·kg^{-1} Pb with 20 g·kg^{-1} $MnFe_2O_4$/SEP (T2), 600 mg·kg^{-1} Pb without $MnFe_2O_4$/SEP (T3), 600 mg·kg^{-1} Pb with 20 g·kg^{-1} $MnFe_2O_4$/SEP (T4), 900 mg·kg^{-1} Pb without $MnFe_2O_4$/SEP (T5), and 900 mg·kg^{-1} Pb with 20 g·kg^{-1} $MnFe_2O_4$/SEP (T6). A control (CK) without Pb^{2+} or $MnFe_2O_4$/SEP was also included. *Brassica chinensis* was selected as the test plant. A uniform amount of compound fertilizer was applied to each pot. After thorough mixing, the soils were equilibrated for one week before sowing. Ten seeds were sown per pot, and seedlings were thinned to five uniform plants after emergence. Soil moisture was maintained at 60% of the water holding capacity by watering every two days. After 60 days of growth, the entire plants were harvested, and fresh weights were measured using an electronic balance. Samples that were not analyzed immediately were temporarily stored at 4 °C for subsequent determination of Pb accumulation, chlorophyll content, MDA concentration, and antioxidant enzyme activities.

For Pb determination, the leaves were oven-dried at 105 °C for 30 min, followed by drying at 65 °C to a constant weight before further processing. The dried samples were then ground into a fine powder and digested with 2 mL of $HClO_4$ and 8 mL of HNO_3 for 12 h. Solutions were filtered through a 0.45 µm syringe filter prior to Pb determination by ICP-MS (Agilent 7500 Agilent Technologies, Inc., Santa Clara, CA, USA) [40]. Chlorophyll content was measured using the spectrophotometric method [9]. The contents of MDA, SOD, POD, and CAT activities were determined using the trichloroacetic acid-thiobarbituric acid (TCA-TBA), nitroblue tetrazolium (NBT) photoreduction, guaiacol, and hydrogen peroxide methods, respectively [9].

3.7. Statistics and Analysis

Isothermal adsorption data were fitted using the Langmuir, D-R model, and Temkin model and adsorption kinetics were analyzed using pseudo-first-order and pseudo-second-order models. Thermodynamic parameters were calculated using the Van't Hoff equation. Detailed equations and models are provided in Supplemental Information (Text S2). Data processing was performed with Microsoft Excel 2019 and SPSS 26. One-way ANOVA followed by Duncan's multiple range test (p = 0.05) was applied to assess significant differences between treatments. Figures were compiled using Origin 2022.

4. Conclusions

These results demonstrated that a SEP-supported $MnFe_2O_4$ composite was effectively synthesized by chemical co-precipitation using SEP as the raw material, as confirmed by SEM-EDS, XRD, FT-IR and XPS analyses. The $MnFe_2O_4$/SEP composite showed enhanced Pb^{2+} adsorption performance compared with pure SEP under various experimental conditions. Thermodynamic analysis indicated that the adsorption process was spontaneous and primarily governed by chemisorption through ion exchange between Pb^{2+} and H^+, with physisorption playing a secondary role. Moreover, the composite demonstrated excellent reusability, maintaining a high Pb^{2+} removal efficiency (85.4%) after five consecutive adsorption–desorption cycles. In Pb-contaminated soils, application of 20 $g \cdot kg^{-1}$ $MnFe_2O_4$/SEP effectively improved soil pH and CEC, reduced Pb bioavailability, and alleviated Pb-induced oxidative stress in *Brassica chinensis*.

Furthermore, due to its high surface area, abundant functional groups, and strong cation-exchange capacity, $MnFe_2O_4$/SEP has the potential to immobilize other heavy metals, such as Cd^{2+} and Cu^{2+}, although further studies are required to confirm its effectiveness and selectivity. Future research should focus on large-scale field trials, long-term stability under variable environmental conditions, and the assessment of potential ecological impacts. Limitations of this study include the controlled laboratory conditions, short-term exposure, and evaluation of only one crop species, which may not fully reflect complex field scenarios. Addressing these aspects will be crucial for practical application in contaminated soils.

Supplementary Materials: The following supporting information can be downloaded at: https://www.mdpi.com/article/10.3390/plants14193077/s1, Calculation of the adsorption capacity of the adsorbents, the Pb^{2+} removal rate, and the Pb^{2+} recovery rate is provided in Text S1. Kinetics and thermodynamics analysis models and function equations is provided in Text S2. The structural characteristics of the SEP and $MnFe_2O_4$/SEP materials are provided in Table S1. The content of each element in SEP and $MnFe_2O_4$/SEP is provided in Table S2. Pseudo-first-order dynamics and pseudo-second-order kinetics parameters for Pb^{2+} adsorption on $MnFe_2O_4$/SEP is provided in Table S3. Comparison of the physico-chemcial characteristics of SEP and $MnFe_2O_4$/SEP. (a, b) SEM images of SEP and $MnFe_2O_4$/SEP; (c, d) EDS images of SEP and $MnFe_2O_4$/SEP; (e) XRD patterns of

SEP, $MnFe_2O_4$, and $MnFe_2O_4$/SEP, and (f) FT-IR spectra of SEP and $MnFe_2O_4$/SEP is provided in Figure S1. Linear fitting of the adsorption process to (a) pseudo-first-order and (b) pseudo-second-order kinetic models is provided in Figure S2.

Author Contributions: Conceptualization, X.D.; methodology, F.G.; formal analysis, L.M.; investigation, F.G., L.M., Y.Z., J.S. and P.Z.; writing—original draft, F.G.; visualization and writing—original draft preparation, L.M.; writing—review and editing, Y.L., Y.Z., J.S., R.B., P.Z., I.L. and X.D.; data curation, F.G. and Y.L.; supervision, X.D.; funding acquisition, I.L. and X.D. All authors have read and agreed to the published version of the manuscript.

Funding: This research was funded by the National Natural Science Foundation of China (41301530) and the National Key Research and Development Program of China (2017YFD0801103). D.X. acknowledges the support of the China Scholarship Council program (202408210317). L.I. acknowledges funding from the Horizon 2020 Marie Skłodowska-Curie Research and Innovation Staff Exchange project CompSafeNano (Grant Agreement No. 101008099).

Data Availability Statement: Data are contained within the article.

Conflicts of Interest: The authors declare no conflicts of interest.

References

1. Singh, O.V.; Labana, S.; Pandey, G.; Budhiraja, R.; Jain, R.K. Phytoremediation: An overview of metallic ion decontamination from soil. *Appl. Microbiol. Biotechnol.* **2003**, *61*, 405–412. [CrossRef]
2. Lei, Q.; Ma, W.; Wang, W. The heavy mental lead pollution progress and control measures of the vegetables in China. *Process. Agric. Prod.* **2012**, *9*, 105–107+124.
3. Gao, R.; Hu, H.; Fu, Q.; Li, Z.; Xing, Z.; Ali, U.; Zhu, J.; Liu, Y. Remediation of Pb, Cd, and Cu contaminated soil by co-pyrolysis biochar derived from rape straw and orthophosphate: Speciation transformation, risk evaluation and mechanism inquiry. *Sci. Total Environ.* **2020**, *730*, 139119. [CrossRef] [PubMed]
4. Lyu, F.; Niu, S.; Wang, L.; Liu, R.; Sun, W.; He, D. Efficient removal of Pb(II) ions from aqueous solution by modified red mud. *J. Hazard. Mater.* **2021**, *406*, 124678. [CrossRef]
5. Jawad, A.; Peng, L.; Liao, Z.; Zhuo, Z.; Shahzad, A.; Ifthikar, J.; Zhao, M.; Chen, Z.; Chen, Z. Selective removal of heavy metals by hydrotalcites as adsorbents in diverse wastewater: Different intercalated anions with different mechanisms. *J. Clean. Prod.* **2019**, *211*, 1112–1126. [CrossRef]
6. Li, Z.; Wang, L.; Meng, J.; Liu, X.; Xu, J.; Wang, F.; Brookes, P. Zeolite-supported nanoscale zero-valent iron: New findings on simultaneous adsorption of Cd(II), Pb(II), and As(III) in aqueous solution and soil. *J. Hazard. Mater.* **2018**, *344*, 1–11. [CrossRef]
7. Zhang, T.; Wang, W.; Zhao, Y.; Bai, H.; Wen, T.; Kang, S.; Song, G.; Song, S.; Komarneni, S. Removal of heavy metals and dyes by clay-based adsorbents: From natural clays to 1D and 2D nano-composites. *Chem. Eng. J.* **2021**, *420*, 127574. [CrossRef]
8. Arshad, F.; Selvaraj, M.; Zain, J.; Banat, F.; Abu haija, M. Polyethylenimine modified graphene oxide hydrogel composite as an efficient adsorbent for heavy metal ions. *Sep. Purif. Technol.* **2019**, *209*, 870–880. [CrossRef]
9. Feng, S.; Zhang, P.; Hu, Y.; Jin, F.; Liu, Y.; Cai, S.; Song, Z.; Zhang, X.; Nadezhda, T.; Guo, Z.; et al. Combined application of biochar and nano-zeolite enhanced cadmium immobilization and promote the growth of Pak Choi in cadmium contaminated soil. *NanoImpact* **2022**, *28*, 100421. [CrossRef] [PubMed]
10. Zhang, L.; Guo, J.; Huang, X.; Wang, W.; Sun, P.; Li, Y.; Han, J. Functionalized biochar-supported magnetic $MnFe_2O_4$ nanocomposite for the removal of Pb(ii) and Cd(ii). *RSC Adv.* **2019**, *9*, 365–376. [CrossRef]
11. Zhan, Y.; Meng, Y.; Li, W.; Chen, Z.; Yan, N.; Li, Y.; Teng, M. Magnetic recoverable MnFe2O4/cellulose nanocrystal composites as an efficient catalyst for decomposition of methylene blue. *Ind. Crop. Prod.* **2018**, *122*, 422–429. [CrossRef]
12. Othman, I.; Abu Haija, M.; Kannan, P.; Banat, F. Adsorptive Removal of Methylene Blue from Water Using High-Performance Alginate-Based Beads. *Water Air Soil Pollut.* **2020**, *231*, 396. [CrossRef]
13. Chen, Y.; Xu, F.; Li, H.; Li, Y.; Liu, Y.; Chen, Y.; Li, M.; Li, L.; Jiang, H.; Chen, L. Simple hydrothermal synthesis of magnetic $MnFe_2O_4$-sludge biochar composites for removal of aqueous Pb^{2+}. *J. Anal. Appl. Pyrolysis* **2021**, *156*, 105173. [CrossRef]
14. Otunola, B.O.; Ololade, O.O. A review on the application of clay minerals as heavy metal adsorbents for remediation purposes. *Environ. Technol. Innov.* **2020**, *18*, 100692. [CrossRef]
15. Fu, R.; Yang, Y.; Xu, Z.; Zhang, X.; Guo, X.; Bi, D. The removal of chromium (VI) and lead (II) from groundwater using sepiolite-supported nanoscale zero-valent iron (S-NZVI). *Chemosphere* **2015**, *138*, 726–734. [CrossRef] [PubMed]

16. Xu, J.; He, J.; Zhu, L.; Guo, S.; Chen, H. A novel utilization of raw sepiolite: Preparation of magnetic adsorbent directly based on sol-gel for adsorption of Pb(II). *Environ. Sci. Pollut. Res.* **2022**, *29*, 77448–77461. [CrossRef]
17. Luo, L.; Wu, H.; Xu, L.; Meng, J.; Lu, J.; Zhou, H.; Huo, X.; Huang, L. An insitu ATR-FTIR study of mixed collectors BHA/DDA adsorption in ilmenite-titanaugite flotation system. *Int. J. Min. Sci. Technol.* **2021**, *31*, 689–697. [CrossRef]
18. Zhang, X.; Zhang, P.; Hu, Y.; Liu, Y.; Feng, S.; Dang, X. Immobilization of cadmium in soil and improved iron concentration and grain yields of maize (*Zea mays* L.) by chelated iron amendments. *Environ. Sci. Pollut. Res.* **2021**, *28*, 53161–53170. [CrossRef]
19. Song, Y.; Wang, N.; Yang, L.Y.; Wang, Y.G.; Yu, D.; Ouyang, X.K. Facile Fabrication of ZIF-8/Calcium Alginate Microparticles for Highly Efficient Adsorption of Pb(II) from Aqueous Solutions. *Ind. Eng. Chem. Res.* **2019**, *58*, 6394–6401. [CrossRef]
20. Antonietta, M.; Olimpia, T.; Federico, R.; Giancarlo, C.; Olga, S.; Michele, P.; Vincenzo, V.; Serena, E. Enhanced adsorptive removal of chloramphenicol from water by highly defective MOF-808 nanocrystals fine-tuned with reliable synthesis strategy: Mechanism insight by equilibrium, kinetics and molecular dynamics simulations. *Chem. Eng. J.* **2025**, *15*, 504.
21. Alexander, E.B.; Evgeny, V.G.; Irina, V.B.; Anastassia, E.K.; Shilpi, A.; Alexey, G.K.; Vinod, K.G. Adsorption of heavy metals on conventional and nanostructured materials for wastewater treatment purposes: A review. *Ecotoxicol. Environ. Saf.* **2018**, *148*, 702–712. [CrossRef] [PubMed]
22. Chen, Y.; Wang, S.; Li, Y.; Liu, Y.; Chen, Y.; Wu, Y.; Zhang, J.; Li, H.; Peng, Z.; Xu, R.; et al. Adsorption of Pb(II) by tourmaline-montmorillonite composite in aqueous phase. *J. Colloid Interface Sci.* **2020**, *575*, 367–376. [CrossRef]
23. Huang, Y.; Luo, X.; Liu, C.; You, S.; Rad, S.; Qin, L. Effective adsorption of Pb(ii) from wastewater using MnO_2 loaded MgFe-LD(H)O composites: Adsorption behavior and mechanism. *RSC Adv.* **2023**, *28*, 19288–19300. [CrossRef] [PubMed]
24. Ghorbani, Y.A.; Ghoreishi, S.M.; Ghani, M. Derived N-doped carbon through core-shell structured metal-organic frameworks as a novel sorbent for dispersive solid phase extraction of Cr(III) and Pb(II) from water samples followed by quantitation through flame atomic absorption spectrometry. *Microchem. J.* **2020**, *155*, 104786. [CrossRef]
25. Vuković, G.D.; Marinković, A.D.; Škapin, S.D.; Ristić, M.D.; Aleksić, R.; Perić-Grujić, A.A.; Uskoković, P.S. Removal of lead from water by amino modified multi-walled carbon nanotubes. *Chem. Eng. J.* **2011**, *173*, 855–865. [CrossRef]
26. Yang, X.; Dai, X.; Jian, T.; Tian, W. Enhanced adsorption and reduction of Pb(II) from aqueous solution by sulfide-modified nanoscale zerovalent iron: Characterization, kinetics and mechanisms. *Inorg. Chem. Commun.* **2024**, *170*, 113496. [CrossRef]
27. Zain, Z.M.; Abdulhameed, A.S.; Jawad, A.H.; ALOthman, Z.A.; Yaseen, Z.M. A pH-Sensitive Surface of Chitosan/Sepiolite Clay/Algae Biocomposite for the Removal of Malachite Green and Remazol Brilliant Blue R Dyes: Optimization and Adsorption Mechanism Study. *J. Polym. Environ.* **2023**, *31*, 501–518. [CrossRef]
28. Wang, C.; Xu, Y.; Wang, L.; Sun, Y.; Liang, X.; Qin, X.; Sun, Y. Immobilization Remediation Effects of Sepiolite and Phosphate on Cadmium and Lead Compound Contaminated Soil. *J. Saf. Environ.* **2010**, *10*, 42–45.
29. Rathika, R.; Srinivasan, P.; Alkahtani, J.; Al-Humaid, L.A.; Alwahibi, M.S.; Mythili, R.; Selvankumar, T. Influence of biochar and EDTA on enhanced phytoremediation of lead contaminated soil by Brassica juncea. *Chemosphere* **2021**, *271*, 129513. [CrossRef]
30. Herbinger, K.; Tausz, M.; Wonisch, A.; Soja, G.; Sorger, A.; Grill, D. Complex interactive effects of drought and ozone stress on the antioxidant defence systems of two wheat cultivars. *Plant Physiol. Biochem.* **2002**, *40*, 691–696. [CrossRef]
31. Cannata, M.G.; Carvalho, R.; Bertoli, A.C.; Augusto, A.S.; Bastos, A.R.R.; Carvalho, J.G.; Freitas, M.P. Effects of Cadmium and Lead on Plant Growth and Content of Heavy Metals in Arugula Cultivated in Nutritive Solution. *Commun. Soil Sci. Plant Anal.* **2013**, *44*, 952–961. [CrossRef]
32. Labidi, S.; Firmin, S.; Verdin, A.; Bidar, G.; Laruelle, F.; Douay, F.; Shirali, P.; Fontaine, J.; Lounès-Hadj Sahraoui, A. Nature of fly ash amendments differently influences oxidative stress alleviation in four forest tree species and metal trace element phytostabilization in aged contaminated soil: A long-term field experiment. *Ecotoxicol. Environ. Saf.* **2017**, *138*, 190–198. [CrossRef] [PubMed]
33. *ISO 10390*; Soil, Treated Biowaste and Sludge—Determination of pH. International Organization for Standardization: Geneva, Switzerland, 2021.
34. Lu, R. *Soil Agrochemistry Analysis Protocols*; China Agriculture Science Press: Beijing, China, 1999.
35. Gao, L.; Sun, Q.; Xu, J.; Liu, B.; Li, J. Explore on Best Digestion Conditions of the United Digestive Solution in Soil. *Chin. Agric. Sci. Bull.* **2012**, *27*, 104–108.
36. Xiang, Y.; Yang, X.; Xu, Z.; Hu, W.; Zhou, Y.; Wan, Z.; Yang, Y.; Wei, Y.; Yang, J.; Tsang, D.C.W. Fabrication of sustainable manganese ferrite modified biochar from vinasse for enhanced adsorption of fluoroquinolone antibiotics: Effects and mechanisms. *Sci. Total Environ.* **2020**, 709. [CrossRef] [PubMed]
37. *GB 15618-2018*; Soil Environmental Quality—Risk Control Standard for Soil Contamination of Agricultural Land. Ministry of Ecology and Environment of the People's Republic of China: Beijing, China; State Administration for Market Regulation: Beijing, China, 2018.
38. Zhang, H.; Wang, Y.; Wang, H.; Ju, W.; Huang, R.; Liu, R.; Du, M. Heavy metal pollution characteristics and health risk assessment of soil from an abandoned site for lead smelting of waste lead batteries. *J. Environ. Eng. Technol.* **2023**, *13*, 769–777.

39. Pardo, R.; Vega, M.; Barrado, E.; Castrillejo, Y.; Sánchez, I. Three-way principal component analysis as a tool to evaluate the chemical stability of metal bearing residues from wastewater treatment by the ferriteprocess. *J. Hazard. Mater.* **2013**, *262*, 71–82. [CrossRef]
40. Filipiak-Szok, A.; Kurzawa, M.; Szłyk, E. Determination of toxic metals by ICP-MS in Asiatic and European medicinal plants and dietary supplements. *J. Trace Elem. Med. Biol.* **2015**, *30*, 54–58. [CrossRef]

Disclaimer/Publisher's Note: The statements, opinions and data contained in all publications are solely those of the individual author(s) and contributor(s) and not of MDPI and/or the editor(s). MDPI and/or the editor(s) disclaim responsibility for any injury to people or property resulting from any ideas, methods, instructions or products referred to in the content.